Analytical and Bioanalytical Chemistry (2022) 414:1359–1373
https://doi.org/10.1007/s00216-021-03758-x

RESEARCH PAPER

Three-dimensional porous calcium alginate fluorescence bead–based immunoassay for highly sensitive early diagnosis of breast cancer

Ying Yao Chia[1] · T. Malathi Theverajah[2] · Yatimah Alias[1] · Sook Mei Khor[1,3]

Received: 15 September 2021 / Revised: 25 October 2021 / Accepted: 27 October 2021 / Published online: 27 November 2021

Abstract

A sensitive biosensor capable of detecting trace concentrations of several cancer biomarkers in clinical samples is critical for early detection of cancer because different cancer biomarkers may be expressed at different stages of cancer. Previous multiplex studies using microarrays or color-coded beads had limited multiplex detection in a single well, and difficulty in optimizing and unifying the incubation parameters for all tests made in different wells had posed challenges to small sample size and lengthened assay time. Herein, we proposed a novel approach to achieve multiplex analysis on a single three-dimensional porous calcium alginate bead. Because of the high surface area to volume ratio of the calcium alginate immuno-bead, the sensitivity and linear dynamic range of the as-proposed multiplex analysis method are significantly improved. Based on the direct sandwich immunoassay principle, dual-capturing antibodies were encapsulated into a single 3D porous calcium alginate bead as a proof-of-concept for multiplexity detection of serum-HER2 and serum-CA125 breast cancer biomarkers. High sensitivity was attained, with LODs of 0.004 ng mL^{-1} for serum HER2, and 0.005 U mL^{-1} for serum CA125, both of which are below the clinical cutoff values, enabling for early breast cancer diagnosis. Stability tests revealed that the 3D immuno-beads were stable at 4 °C and room temperature (25 °C) for at least 14 days. Most importantly, the results obtained using the developed system were in good agreement with those obtained using standard methods while analyzing real clinical samples. In addition, the analysis required only approximately 30 min, which was much less time than typical ELISA techniques. When endogenous interferences were introduced, no cross-reactivity was observed. We anticipate this approach to be potentially used in the multiplex assays and biosensors.

Keywords Breast cancer · Multiplexed immunoassay · HER2 · CA125 · Calcium alginate bead · Sandwich immunoassay

Introduction

Breast cancer is a non-contagious disease consisting of an abnormal proliferation of cells within the breast tissues, arising from the breast lobules or milk ducts [1]. Every year, approximately 2.1 million women are diagnosed with breast cancer globally. It has been classified as the most common cancer worldwide, which affects both sexes from all ethnicities, with the highest incidence observed in American women [2–4]. Women are 100 times more prone to the disease than men; however, men often receive a poor diagnosis because of the lack of awareness or delayed prognosis [5]. In Malaysia, breast cancer was accounted for 17% of the total 43,837 cancer cases in 2018. In the same year, 11% out of a total of 26,395 cancer-related deaths were associated with breast cancer [6]. According to Blue Code news website, statistics from the Malaysia National Cancer Registry report revealed that Chinese women in Malaysia have a higher risk of cancer than other ethnic groups like Indians, followed by Malays [7]. In addition, with an increase in age, the risk of acquiring the disease increases [8, 9]. In general, lower morbidity rates have been observed in Asian countries than in Western countries. However, because Asian countries have low-to-middle-low socioeconomic status, expensive routine medical checkups and general medical attention could be burdening. Consequently, Asian countries tend to have

✉ Sook Mei Khor
naomikhor@um.edu.my

[1] Department of Chemistry, Faculty of Science, University of Malaya, 50603 Kuala Lumpur, Malaysia

[2] Department of Pathology, Faculty of Medicine, University of Malaya, 50603 Kuala Lumpur, Malaysia

[3] Centre for Innovation in Medical Engineering, Faculty of Engineering, University of Malaya, 50603 Kuala Lumpur, Malaysia

higher mortality rates. Such circumstances persist despite knowledge promotion on "early cancer detection is the main key to cure" [10, 11].

The gold standard for breast cancer diagnosis, which comprises mammography, ultrasound, physical examination, and cellular packaging analysis, cannot be disregarded. However, the majority of these methods are costly, invasive, expose patients to radiation, lack sensitivity or specificity, or are limited to a specific part of the tumor [12–14]. Unlike blood biochemistry analysis adopting ELISA or modified ELISA-based detection method in laboratory, ELISA allows quantitative measurement of trace biomarkers in blood that made early breast cancer detection possible due to their high sensitivity, specificity, and cost-effectiveness [15]. Unfortunately, such a method is time-consuming, and multiplex detection in a single well is unlikely due to color signals overlapping as a result of multiple enzyme–substrate reactions [16, 17], but fluorescent detection can do the trick because different fluorophores have their own distinct emission profiles [18], allowing simultaneous detection of multiple cancer biomarkers.

Tumor biomarkers are liquid-soluble substances that are released by the tumor cells to its surroundings, such as body fluid, sputum, blood serum, and urine. Such aberrations could indicate its hyperactivity, gene alterations, or cell–cell communications in the forms of proteins, enzymes, receptors, antibodies, nucleic acids, growth hormones, and exosomes [19–22]. Often, the quantity of the tumor biomarkers released into the body fluids is scarce at the initial stage and increases gradually with the progress of cancer [23]. Furthermore, different tumor biomarkers may be expressed at different stages of cancer [24]. Hence, a sensitive biosensor that is capable of detecting trace concentrations of multiple tumor markers in clinical samples is important for the diagnosis of early onset of the disease [25–28]. Table 1 summarizes the advantages, disadvantages, challenges, and limitations of optical biosensors that have been reported to diagnose breast cancer using various optical transducers in recent years. In overview, the majority of the approaches listed in the table only support single biomarker detection [12, 29–36], while those that enable multiplex detection either required complex fabrication processes [37] or biosensor sensitivity deteriorated when multiplexed biomarkers were detected in the actual serum sample, limiting their application in clinical settings [38]. When it comes to the widely known multiplexed immunosensor format, such as microarray and color-coded beads in well plates, one disadvantage is that each test well or color-coded bead can only carry a single biorecognition molecule or probe, resulting in a small sample volume that may be insufficient for sensitive and accurate analysis since multiplexed detection required multiple color beads [39]. In terms of assay duration, Elakkiya and co-researchers achieved the shortest assay time of 15 min with their fluorescent immunoassay [36], while the longest assay time was more than 390 min [29].

Most reports on biosensor-based diagnosis of breast cancer and cancer-related diseases focused on the sensitivity of the biosensors in an attempt to improve the analytical performance of the detection. For this purpose, researchers have used nanomaterials such as gold nanoparticles [41, 42], silver nanoparticles [43, 44], magnetic beads [45, 46], and quantum dots [47], and heavy metals such as cadmium sulfide [48] and aluminum nitrite [49] incorporated with recognizing bio-moieties, such as aptamers or antibodies, which can be disadvantageous in some cases because they involve complicated and lengthy processes of surface passivation, as well as diffusion or chemisorption of the proteins onto the surface of the nanoparticles. Furthermore, protein denaturation may occur as a result of protein adsorption onto hydrophobic bulk surfaces due to reorganization of the protein's water molecules, resulting in a reduction in the yield of readily available functional capturing elements to the target analyte [50, 51]. Furthermore, the use of heavy metals may have a detrimental impact on the health of researchers, users, the environment, and marine life upon disposal [52–56]. In contrast, using a 3D porous calcium alginate bead as a medium for entrapment of biorecognition molecules during ionotropic gelation in the presence of divalent calcium cations that happened in a click of time could significantly reduce the time and cost required for mass production [57]. Unlike other hydrogels, such as agarose gel, wherein the encapsulation of biomaterials within the structure decreases the strength of the gel and imparts fragility, calcium cross-linked alginate beads remain stable [58]. Moreover, the bioactivity of the biomolecules or bioreceptors entrapped in the porous network of the calcium alginate beads could be preserved, owing to the biocompatibility of the calcium alginate beads [59]. In addition, calcium alginate beads have pore sizes ranging from 0.00001 to 100 nm. The 3D porous calcium alginate beads have a large surface area to volume ratio, which allows for high-yield entrapment of biorecognition molecules as well as the entrance and exchange of fluids within and outside the porous beads. Hence, they have been frequently reported as cell scaffolds and drug carriers designed for a sustained release [60, 61]. Because of the macroscopic semi-transparent appearance of the 3D porous calcium alginate beads, we hypothesize their potential use in multiplex assays, which allow the penetration of light and enable multiplex fluorescence quantification of breast cancer biomarkers within a single bead. Multiplex biomarker detection is essential to improve the accuracy and specificity of early diagnosis because of the heterogeneity nature of breast cancer [57].

To fill in the research gap, herein, we report the first example of the calcium alginate immuno-bead comprising two biorecognition elements (anti-HER2 monoclonal

Table 1 Comparison of the optical biosensors reported for the detection of breast cancer biomarkers

Breast cancer biomarker(s)	Biorecognition element(s)/bioreceptor(s)	Type of sample	Detecting element(s)	Optical transducer	Limit of detection (LOD)/linear range	Detection time	Advantage(s)	Disadvantage(s)/challenge(s)/limitation(s)	References
• Estrogen receptor (ERα)	• ERα proteins extracted directly from the samples	• MCF-7 and MDA-MB-231 cell line	• Primary anti-ERα antibody and secondary Alexa™ Fluor 488 or 555 labeled goat anti-rabbit IgG antibody	• Photonic crystal	• 20 pg	• < 390 min	• Sensitive	• Invasive method to obtain cellular material is required for testing Complex sample pre-treatment processes	[29]
• miR-155	• C-AuNPs coated with thiolated hairpin capture probe DNA	• P-AuNPs coated with miR-155 in deionized water	• Hybridization of a C-AuNP capturing probe with a P-AuNP-coated miR-155 results in aggregation	• Colorimetric	• 10 aM to 100 fM	• < 50 min	• Sensitive	• Not tested with clinical samples Could only detect one biomarker	[12]
• HER2 ECD protein	• Anti-HER2 capturing antibody	• HER2 ECD protein spiked in PBS • Human serum samples	• Streptavidin-linked ALP conjugated biotinylated anti-HER2 detecting antibody	• Colorimetric	• 0.5 ng mL^{-1} (naked eye observation) • 0.05 ng mL^{-1} (UV–vis detection)	> 360 min	• Sensitive • Allow visual observation of color change	• Lengthy assay time • Could only detect one biomarker • Involving multiple washing steps	[30]
• Human anti-GIPC-1 IgM autoantibody (27.B1)	• GIPC-1 protein	• Human serum samples	• Horseradish peroxidase-labeled goat anti-human IgM antibody	•Chemiluminescence	• 30 pg mL^{-1}	• > 150 min	• Sensitive	• Could only detect one biomarker Multiple and lengthy washing steps	[31]
• HER2 protein	• Mouse monoclonal IgG antibody-Neu (*ER23*)	• HER2 protein spiked in PBS Human serum samples	• N/A	• Resonator	• 13 to 100 ng mL^{-1}	• < 30 min	• Rapid and label-free detection	• Could only detect one biomarker	[32]
• CA15-3 protein	• Anti-CA15-3 antibody	• CA15-3 protein spiked in PBS • Human serum samples	• N/A	• Resonator	• 1 U mL^{-1}	• < 30 min	• Rapid and label-free detection	• Could only detect one biomarker	[33]

Table 1 (continued)

Breast cancer biomarker(s)	Biorecognition element(s)/bioreceptor(s)	Type of sample	Detecting element(s)	Optical transducer	Limit of detection (LOD)/linear range	Detection time	Advantage(s)	Disadvantage(s)/challenge(s)/limitation(s)	References
• CA15-3 protein • CA125 protein • CEA	• Anti-CA15-3 antibody • Anti-CA125 antibody Anti-CEA	• Protein biomarker(s) spiked in PBS • Human serum samples	• SERS probe–conjugated anti-CA153 • SERS probe–conjugated CA125 • SERS probe–conjugated anti-CEA	• SERS	• CA15-3: 0.01 U mL^{-1} • CA125: 0.01 U mL^{-1} • CEA: 1 pg mL^{-1}	• > 75 min	• Enable multiplex quantification	• 100-fold decreased in sensitivity when CA15-3 was spiked in serum sample	[37]
• HER2 protein	• Anti-HER2 antibody	• HER2 protein spiked in PBS	• N/A	• Interferometer	• 2 ng mL^{-1}	• > 60 min	• Label-free detection	• Could only detect one biomarker Not tested with real clinical samples	[34]
• HER2 protein	• Anti-HER2 monoclonal antibody	• HER2 protein spiked in aqueous solution	• Secondary anti-HER2 antibody	• SPR	• 3 ng mL^{-1}	• > 60 min	• Label-free detection	• Could only detect one biomarker Not tested with real clinical samples	[35]
• miR-195 let-7a	• miR-195 complementary sequence • let-7a complementary sequence	• Human serum samples	• QD 655-labeled miRNA-195 supporter sequence QD 705-labeled let-7a supporter sequence	• Fluorescence	• miR-195: 0.064 nM • let-7a: 0.061 nM	• > 30 min	• Enable multiplex quantification	• Complex fabrication processes	[38]
• CA15-3	• Anti-CA15-3	• CA15-3 protein spiked in saline • Human serum sample	• Cys-CdS QD-labeled anti-CA15-3	• Fluorescence	• 0.002 KU L^{-1}	• > 15 min	• Sensitive	• Could only detect one biomarker • Did not mention if washing step is necessary	[36]
• Survivin mRNA	• Oligonucleotide sequence targeting mRNA of surviving	• cDNA MCF-7 live cells	• FAM-labeled at the 3′ of the capturing oligonucleotide sequence	• Fluorescence	• 3 nM	• > 12 h	• Sensitive	• Involving time-consuming steps Could only detect one biomarker	[40]

Table 1 (continued)

Breast cancer biomarker(s)	Biorecognition element(s)/bioreceptor(s)	Type of sample	Detecting element(s)	Optical transducer	Limit of detection (LOD)/linear range	Detection time	Advantage(s)	Disadvantage(s)/challenge(s)/limitation(s)	References
• HER2 protein CA125 protein	• Anti-HER2 monoclonal IgG antibody • Anti-CA125 monoclonal IgG antibody	• Biomarker(s) spiked in TBS • Human serum samples	• FITC-labeled anti-HER2 polyclonal IgG antibody • Cy-5-labeled anti-CA125 polyclonal IgG antibody	• Fluorescence	• HER2 protein: 0.004 ng mL^{-1} • CA125 protein: 0.005 U mL^{-1}	< 30 min	• Simple fabrication process • Rapid detection • Enable multiplex quantification • Sensitive	• Require simple rinsing steps to get rid of non-specific proteins from serum sample	This study

IgG capturing antibody and anti-CA125 monoclonal IgG capturing antibody) to target two breast cancer biomarkers (HER2 and CA125 proteins) in a single bead. As a proof-of-concept, the study utilized spiked and real clinical human serum samples to assess the overall analytical performance of multiplex detection potential in a single 3D porous calcium alginate immuno-bead (Scheme 1). Elevated serum HER2 levels are frequently associated to poor prognosis or cancer recurrence [62, 63], whereas elevated CA125 levels could predict metastatic breast cancer [64]. The analytical performance of the 3D calcium alginate immuno-bead-based assay to detect ultra-trace concentrations of serum-HER2 and serum-CA125 concurrently was examined to demonstrate its practicality and reliability. Standard methods, such as enzyme-linked immunosorbent assay (ELISA) and chemiluminescent microparticle immunoassay (CMIA), that was carried out by a commercial BP laboratory in Malaysia were used to verify the results obtained from the examination of clinical samples utilizing the developed methodology. We anticipate this approach to be potentially used in the multiplex assays and biosensors.

Experimental section

Materials and chemicals

Chemicals such as alginic acid sodium salt, TRIZMA hydrochloride, Tween-20, fluorescein isothiocyanate isomer I (FITC), bovine serum albumin (BSA), human serum albumin (HSA), silicon nanoparticles (< 30 nm), and Western blocking (WB) reagents were purchased from Sigma-Aldrich; cyanine 5 NHS ester from Enzo Life Sciences, calcium chloride ($CaCl_2$) from Merck, and sodium chloride from Friendemann Schidmt. Anti-HER2 monoclonal IgG antibody, HER2 protein, anti-HER2 polyclonal IgG antibody, anti-CA125 monoclonal IgG antibody, CA125 protein, and CA125 polyclonal IgG antibody were purchased from Fitzgerald, USA. ErbB2 (HER2/Neu protein) ELISA test kit was purchased from ABCAM, UK.

Synthesis of the 3D porous calcium alginate immuno-beads

The concentrations of the capturing antibodies to be encapsulated into the 3D porous calcium alginate beads were pre-optimized using electrochemical impedance spectroscopy (EIS). Based on the highest resistivity obtained, 60 ng mL^{-1} of anti-HER2 and 20 ng mL^{-1} of anti-CA125 capturing monoclonal IgG antibodies were chosen (described under S2 in the ESM). The two pre-optimized concentrations of the capturing antibodies were mixed with 1.5% sodium alginate dissolved in

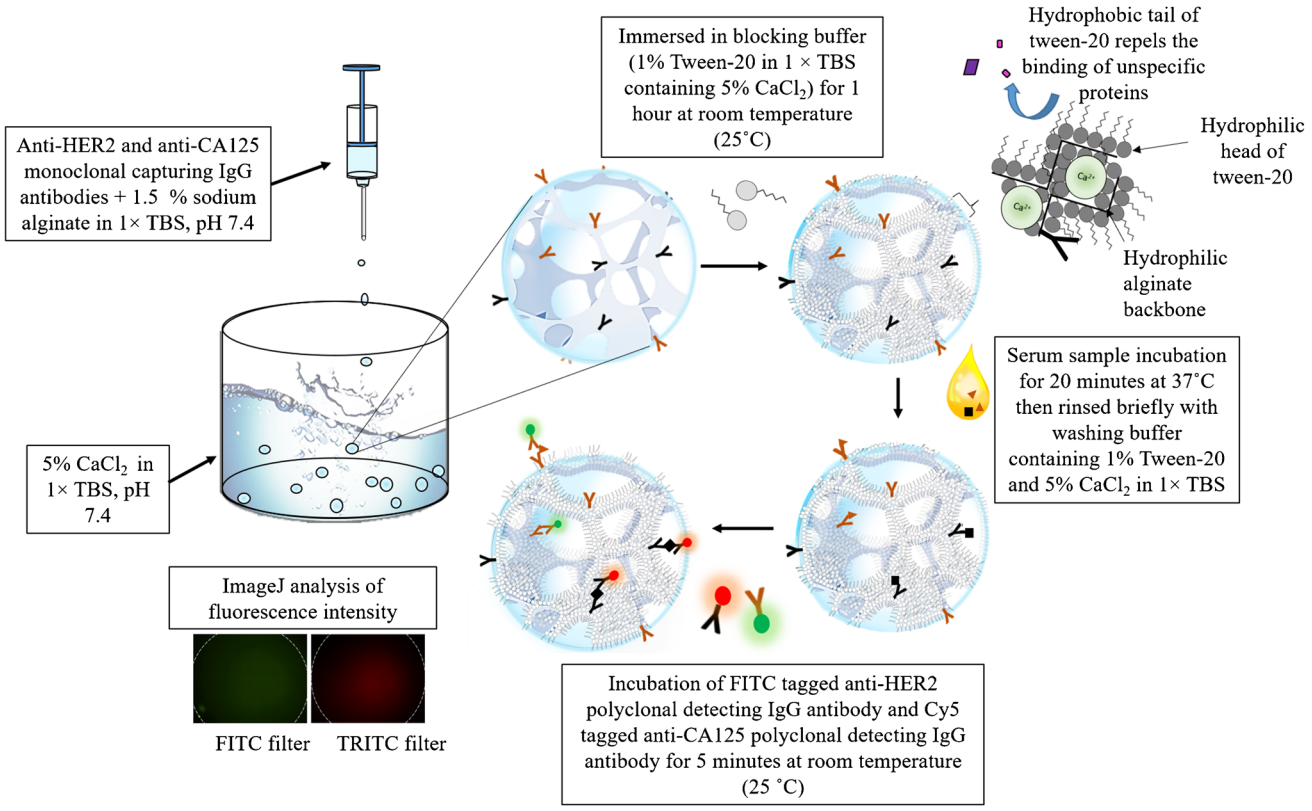

Scheme 1 Stepwise fabrication of the 3D porous calcium alginate immuno-beads for early sensitive detection of breast cancer biomarkers

1 × Tris buffer saline (TBS), at a pH of 7.4. The mixture was then filled into a syringe using a 22G′ bevel needle and introduced into a beaker dropwise with approximately 2 cm above the water level (placed in a bath) containing 1 × TBS and 5% $CaCl_2$, at a pH of 7.4. The mixture was then allowed to sit in the bath for 30 min. Finally, each 3D porous calcium alginate immuno-bead was placed in a separate well in a transparent U-bottom 96-well plate containing 100 µL of storage buffer (1 × TBS and 5% $CaCl_2$, pH 7.4) at 4 °C, to prevent drying of the beads during storage. Note: TBS was used instead of PBS because phosphate in PBS may react with $CaCl_2$ to form less soluble calcium phosphate, causing a white precipitate.

Morphology and structure characterization

The size of the 3D calcium alginate immuno-beads was measured using a measuring caliper. Furthermore, their morphology was characterized using Fourier-transform infrared spectroscopy (FTIR) after drying the samples on glass slides, and field emission scanning electron microscopy (FESEM), after the freeze-drying processes. The internal pore size of the 3D calcium alginate immuno-beads was analyzed using the FESEM images.

Surface blocking to resist unspecific protein binding

The 3D calcium alginate immuno-beads were soaked in the wells of a transparent U-bottom 96-well plate containing 100 µL of 1% Tween-20 in 1 × TBS, and 5% $CaCl_2$ at a pH of 7.4, for 1 h at room temperature (25 °C). Next, the treated calcium alginate immuno-beads were submerged in the storage buffer prior to further treatments. Optimization details of the blocking reagents for Tween-20, WB, silicon nanoparticles, and BSA are elaborated in S3 in the ESM. The blocked 3D calcium alginate immuno-beads were treated with HSA (positively charged protein) and cytochrome C (negatively charged protein) that were tagged with FITC reporter dye to evaluate the antifouling property of the blocking agents. The method of conjugating HSA and cytochrome C with FITC dye was modified from a previous report [65].

Conjugation of anti-HER2 polyclonal IgG antibody to green fluorescence-emitting dye (fluorescein isothiocyanate isomer (FITC)) and anti-CA125 polyclonal IgG antibody to orange-red fluorescence-emitting dye (cyanine 5 (Cy-5))

FITC and Cy-5, which are readily available, have excitation and emission profiles compatible with the fluorescence filter

cubes equipped in Nikon Eclipse fluorescence microscopy (Ti-S). Both dyes were employed as reporter dyes to be conjugated with the detecting antibodies. First, 100 ng mL^{-1} of desalted anti-HER2 detecting polyclonal IgG antibody was mixed with 0.257 µL of the FITC dye; the dye was taken from the stock solution having a concentration of 6.07 ng μL^{-1}, dissolved in 1 × TBS containing 25% v/v DMSO. The mixture was allowed to mix continuously for 1 h in the dark using an orbital shaker at 100 rpm; the mixture was then dialyzed against 1 × TBS, at a pH of 7.4. Similarly, 100 ng mL^{-1} of desalted anti-CA125 detecting polyclonal IgG antibody was mixed with 0.802 µL of the Cy-5 dye; the dye was taken from the stock solution having a concentration of 3.8 ng μL^{-1}, dissolved in 1 × TBS containing 25% v/v DMSO. After 1 h of constant mixing in the dark on a rotator at 100 rpm, the conjugates were dialyzed against 1 × TBS at a pH of 7.4. Finally, both conjugates were analyzed using a UV–vis spectrometer (NanoDrop 2000c, Thermo Scientific) and stored at 4 °C.

Image acquisition using fluorescence microscopy and their analysis using ImageJ software

All fluorescence images were obtained using Nikon Eclipse fluorescence microscopy (Ti-S) under a 4 × magnification objective lens. A Nikon FITC fluorescent filter cube was used to capture the signals emitted from the FITC probes. However, considering the availability of the filter cubes, and compatibility of Cy-5 dye with the Nikon TRITC filter cube (which consists of an excitation range of 540/25 nm and emission at 605/55 nm), a TRITC filter cube was used to capture the signals emitted from the Cy-5 probes. To avoid bias, a similar light exposure setting was employed in image acquisition, by adjusting the gamma light exposure at a random value of 0.62 throughout the experiments. Quantitative analysis of the fluorescence intensity (mean gray value) was performed using ImageJ software (NIH, Bethesda, MD, USA).

Immunoassay using the 3D calcium alginate immuno-beads

Storage buffer was first removed from the well by sucking the solution out of the well with a micropipette to avoid contacting the immuno-bead. One hundred microliters of HER2- and/or CA125-spiked samples or 25% clinical human serum samples diluted with 1 × TBS were then introduced to the 3D calcium alginate immuno-beads placed in the wells of a transparent U-bottom 96-well plate (with only one bead in a well). The antibody-antigen reaction was allowed to take place at 37 °C for 20 min. Then, the reaction mixtures in the wells were rinsed using a washing buffer containing 1% Tween-20 in 1 × TBS and 5% w/v $CaCl_2$. Next, 100 µL of both, 2 ng mL^{-1} solution of FITC-conjugated anti-HER2-, and 10 ng mL^{-1} solution of Cy-5-conjugated anti-CA125-polyclonal IgG antibody detecting probes, was added to the 3D calcium alginate immuno-beads (concentration optimization of the labeled detecting antibodies is described in S3 in the ESM). The 3D porous calcium alginate immuno-beads were then incubated for 5 min at room temperature (25 °C) (incubation time optimization is described in S5, and data summarized in Fig. S6 in the ESM). A final rinse using the washing buffer was done prior to image acquisition using Nikon fluorescence microscopy and quantitative analysis using ImageJ software as described in "Image acquisition using fluorescence microscopy and their analysis using ImageJ software."

Quantitative measurement of breast cancer biomarkers

Two sets of 3D calcium alginate immuno-beads were spiked with serial concentrations of breast cancer biomarkers in separate wells of a transparent U-bottom 96-well plate ($n = 3$ for each concentration), i.e., 0, 2, 5, 8, 10, 15, 30, 45, 60, and 75 ng/mL of HER2 protein, and 0, 2, 5, 8, 10, 15, 30, 45, and 60 U/mL of CA125 protein, spiked in 25% human serum samples which were diluted using 1 × TBS. After the incubation and rinsing processes were performed as described in "Immunoassay using the 3D calcium alginate immuno-beads," the fluorescence images of the 3D porous calcium alginate immuno-beads were captured and analyzed, as described in "Image acquisition using fluorescence microscopy and their analysis using ImageJ software." The linear range at which the signal is proportional to the concentration of the target analyte (HER2 protein and/or CA125 protein) was recorded using the line graph feature of Microsoft Excel. The LOD was calculated using the following formula (Eq. (1)), where LOD can be calculated by multiplying 3.3 with the SD (standard deviation) of the intercept, divided with the slope of the regression line.

$$\mathrm{LOD} = 3.3 \times \frac{\text{SD of intercept}}{\text{slope}} \tag{1}$$

Simultaneous multiplex detection of HER2 and CA125 proteins spiked in serum samples containing complex matrices (n = 3)

The 3D porous calcium alginate immuno-beads were treated with 30 ng mL^{-1} of HER2 protein and 50 U mL^{-1} of CA125 protein, simultaneously, in the wells of a transparent U-bottom 96-well plate. The incubation and rinsing processes were performed using the protocol described in "Immunoassay using the 3D calcium alginate immuno-beads," followed

by image acquisition and analysis as described in "Image acquisition using fluorescence microscopy and their analysis using ImageJ software." Relative standard deviation (RSD) was calculated using the following formula (Eq. (2)), where RSD can be determined by dividing σ (standard deviation of the test result from the replicates) against the mean, followed by multiplication with 100.

$$\mathrm{RSD} = \frac{\sigma}{\mathrm{mean}} \times 100 \quad (2)$$

Precision and recovery test (n = 3)

The degree of closeness between the data obtained within the day (intra-day) and between 3 random days (inter-day) was measured to ensure the precision of the newly developed method. First, the 3D porous calcium alginate immuno-beads were placed in the wells of a transparent U-bottom 96-well plate containing 25% human serum spiked with various concentrations (low, medium, and high) of the HER2 (10, 30, and 50 ng mL^{-1}) and CA125 proteins (10, 30, and 50 U mL^{-1}), simultaneously. After the incubation and rinsing processes were performed as mentioned in "Immunoassay using the 3D calcium alginate immuno-beads," the fluorescence images of the 3D porous calcium alginate immuno-beads were captured and analyzed as described in "Image acquisition using fluorescence microscopy and their analysis using ImageJ software." The percentage of recovery was calculated using the following formula (Eq. (3)), where recovery (%) can be determined by dividing found concentration of target analyte by spiked concentration of the target analyte, followed by multiplication with 100.

$$\text{Recovery } (\%) = \frac{\text{found concentration of target analyte}}{\text{spiked concentration of target analyte}} \times 100 \quad (3)$$

Selectivity and interference test (n = 3)

To ensure that the bioreceptors and detecting antibodies used in the currently developed 3D porous calcium alginate bead–based assay are specific to their own target analyte, a selectivity test was conducted by introducing single or both antigens concurrently where 25 ng mL^{-1} of HER2 protein and 25 U mL^{-1} of CA125 protein were used. After all the incubation and rinsing steps were performed as described in Sect. 2.7, the fluorescence images of the beads were captured and analyzed as described in Sect. 2.6.

Next, to determine if endogenous proteins do interfere with the multiplex quantification of breast cancer biomarkers, 4 mg dL^{-1} of BSA, 6.25 mg dL^{-1} of uric acid, 1.3 mg dL^{-1} of ascorbic acid, and 0.06 ng mL^{-1} of biotin were spiked separately with dual breast cancer biomarkers together (25 ng mL^{-1} of HER2 and 25 U mL^{-1} of CA125 protein) into 25% of human serum. After the incubation and rinsing steps as mentioned in "Image acquisition using fluorescence microscopy and their analysis using ImageJ software," the fluorescence images of the beads were captured and analyzed as described in "Image acquisition using fluorescence microscopy and their analysis using ImageJ software."

Stability test

The performance stability of the monoclonal IgG capturing antibodies encapsulated in the 3D porous calcium alginate immuno-beads after storage at 4 °C and at room temperature (25 °C) was assessed over 14 days, specifically on days 1, 3, 5, 7, and 14 in simultaneous detection 25 ng mL^{-1} of HER2 protein and 25 U mL^{-1} of CA125 protein which were spiked into the 25% human serum samples (n = 3).

Real sample analysis and method verification using standard methods

Ten clinical archived patients' serum samples were obtained from the University of Malaya Medical Centre (UMMC) that had been confirmed with breast cancer. All samples were obtained from female subjects, with ages ranging from 45 to 74 years. The quantification competency of the 3D porous calcium alginate immuno-beads was compared with two gold standard methods, i.e., commercialized ELISA test kit for serum HER2 and serum CA125 was tested using an Abbott Architect ci8200 analyzer that uses CMIA, the gold standard method used by the BP healthcare center. Each serum sample ($n = 10$) to be tested using the 3D porous calcium alginate immuno-bead was diluted with 1 × TBS to obtain 25% serum samples. After the immunogenic reactions were completed and sandwiched between the detecting probes, fluorescence images were captured and analyzed as described in "Image acquisition using fluorescence microscopy and their analysis using ImageJ software." The recovered concentration was calculated by substituting the mean fluorescence intensity value to "y" of the equation obtained from the calibration curve, i.e., $y = mx + c$, where y is the fluorescence intensity, m is the slope, x is the concentration of the target analyte, and c is the fluorescence intensity observed when $x = 0$. Because the serum samples were fourfold diluted for the assay, the calculated concentrations were multiplied by 4 to obtain the concentration of the biomarker in the undiluted serum samples.

Results and discussion

Characterization

Characterization of 3D porous calcium alginate immuno-beads

Inverted light microscopy, FESEM, and FTIR were used to confirm the successful synthesis of the 3D porous calcium alginate immuno-beads. Few optimization parameters were performed beforehand, such as that of concentration of sodium alginate (Fig. S1), the concentration of the capturing antibodies to be encapsulated in a single calcium alginate bead (Fig. S2) and blocking reagents (Fig. S3). From the phase-contrast images obtained using the inverted light microscopy (Fig. 1a and b), a single 3D porous calcium alginate immuno-bead appeared to have a smooth and round appearance with a complex branch-like internal structure which could be vaguely visualized through the shades. The morphology of the 3D porous calcium alginate immuno-bead was further analyzed via FESEM. From Fig. 1c and d of the FESEM images, the surface texture of the 3D porous calcium alginate immuno-bead was found to be relatively rough compared to its appearance in the phase-contrast images. In the FESEM images of the cross-sectional sample shown in Fig. 1e and f, the internally cross-linked network exhibited varying sizes of rhombic pores ranging from 0.022 to 196 nm. Such a feature is mandatory for fluid exchange in the proposed system. Despite the fact that the pores vary in size, it is abundant. Given that the size of the immuno-sandwich formed by the capturing antibody ($\pm$ 14.5 nm × 8.5 nm × 4.0 nm) that has been encapsulated inside the structure, the target analytes: HER2 (185 kDa, approx. 5.6 nm) and CA125 (700 kDa, approx. 21.4 nm) and detecting antibody ($\pm$ 14.5 nm × 8.5 nm × 4.0 nm), are only less than about 60 nm regardless of their orientation; therefore, the diluted serum sample (with less viscosity) containing biomolecules as well as the detecting antibody could gain entry from different angles since the pores are readily accessible all over the surfaces of a 3D porous calcium alginate immuno-bead and thus for fluid exchange. By adjusting the calcium chloride concentration, the number of pores and pore sizes of the calcium alginate immuno-bead can be customized. Increases in the number of holes could increase the number of immobilized capturing antibodies, improving the sensitivity of the immunoassay. Further narrowing of the pores, on the other hand, may obstruct the features of the current system, such as antigen–antibody binding and liquid flow. Additionally, the FTIR spectra (Fig. 1g) showed a red shift of the C = O peak from 1720 cm^{-1} to a lower wavenumber at 1634 cm^{-1}, which confirms the bond between the carboxyl group of sodium alginate and calcium ions in the $CaCl_2$ solution. The N–H-attributed peak at 1629 cm^{-1} and 821 cm^{-1} confirmed the successful encapsulation of the capturing antibodies within the 3D porous calcium alginate bead-structure; however, N–H-associated peaks were not identified between 3300 and 3500 cm^{-1}, which may be most probably caused by the strong intensity of the O–H peak which appeared at 3345^{-1} cm that has obscured the N–H peaks and rendered than insignificant. Besides, flattening or diminishing peaks were seen after the treatment with a 1% Tween-20 blocking reagent, which confirms the successful absorption of the blocking agent within the 3D porous calcium alginate immuno-beads.

Characterization of conjugates

FITC-conjugated anti-HER2- and Cy-5 conjugated anti-CA125-polyclonal IgG–detecting antibodies were characterized using UV–Vis spectrometry. As shown in Fig. S4, a notable redshift was seen after conjugation, indicating successful conjugation because of the size increment. Fig. S5 in the ESM shows the optimum concentrations of conjugates/labeled detecting antibodies used in the experiments were found to be 2 ng mL^{-1} for FITC-conjugated anti-HER2 polyclonal IgG–detecting antibody and 10 U mL^{-1} for Cy-5 conjugated anti-CA125 polyclonal IgG–detecting antibody.

Standard curve for quantitative assay

A calibration curve, also known as a standard curve, is a regression model for determining the concentration of an unknown sample. A calibration curve was plotted (Fig. 2) using the mean gray value obtained from the images (Fig. S7a and b) generated by ImageJ software. Linear regression was observed for the serum samples spiked with HER2 and CA125 biomarkers with $R^2 = 0.972$ (Fig. 2a) and 0.982 (Fig. 2b), respectively. The calculated LODs for serum sample spiked with HER2 was 0.004 ng mL^{-1} (cutoff point: > 15 ng mL^{-1}), and 0.005 U mL^{-1} (cutoff point > 35 U mL^{-1}) for the serum sample spiked with CA125, which was much lower than the clinical cutoff values. When both target analytes were spiked concurrently into the serum sample, the linear regression for the detection of HER2 was $R^2 = 0.969$ (Fig. 2c) and $R^2 = 0.978$ (Fig. 2d) for CA125. Although the obtained LODs were slightly higher than those obtained from single spiked samples (with only 0.008 ng mL^{-1} for HER2 and 0.011 U mL^{-1} for CA125 being detected), however, the obtained values for HER2 and CA125 were still far below the clinical cutoff values, with good sensitivity over a linear range of 0–10 ng mL^{-1} and 0–10 U mL^{-1} for the detection of HER2 and CA125, respectively (single

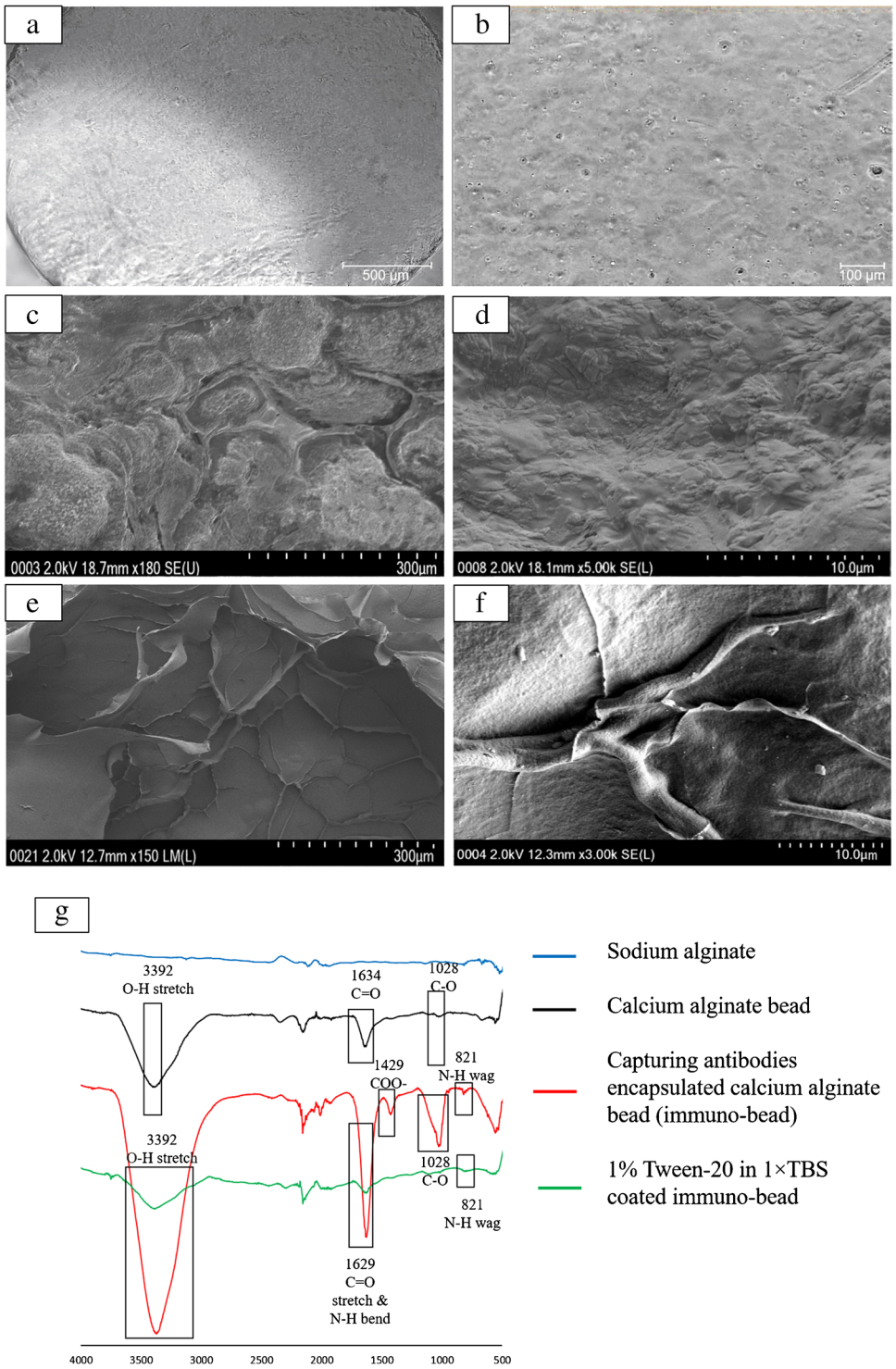

Fig. 1 Phase-contrast images of a 3D porous calcium alginate immuno-bead at **a** 4× magnification; **b** 10× magnification; **c** FESEM surface image of the freeze-dried 3D porous calcium alginate immuno-bead; **d** FESEM zoomed-in surface image of the freeze-dried 3D porous calcium alginate immuno-bead; **e** FESEM cross-sectional image of the freeze-dried 3D porous calcium alginate immuno-bead; **f** FESEM zoomed-in cross-sectional image of the freeze-dried 3D porous calcium alginate immuno-bead; and **g** FTIR spectra for sodium alginate (blue line), calcium alginate bead (black line), capturing antibodies encapsulated calcium alginate bead, also known as a 3D porous calcium alginate immuno-bead (red line) and 1% Tween-20 blocking agent coated on a 3D porous calcium alginate immuno-bead (green line). Note: All FTIR samples were pre-dried onto the surface of glass slides prior to analysis

or simultaneous spiked). Table 1 compares the sensitivity of the HER2 and CA125 detection in this study to that of other published studies. Serum HER2 and serum CA125 levels as low as 0.05 ng mL^{-1} and 0.01 U mL^{-1}, respectively, have been reported. It is worth mentioning that, when compared to published data, the detection sensitivity of serum HER2 employing the 3D porous calcium alginate immuno-bead-based assay has improved even more, but CA125 has remained unchanged.

Additionally, to confirm whether non-specific absorption of the detecting antibody into the 3D porous calcium alginate immuno-bead occurs, two negative control studies, one in the presence of the detecting antibody and absence of the target analyte, and the other in the absence of the

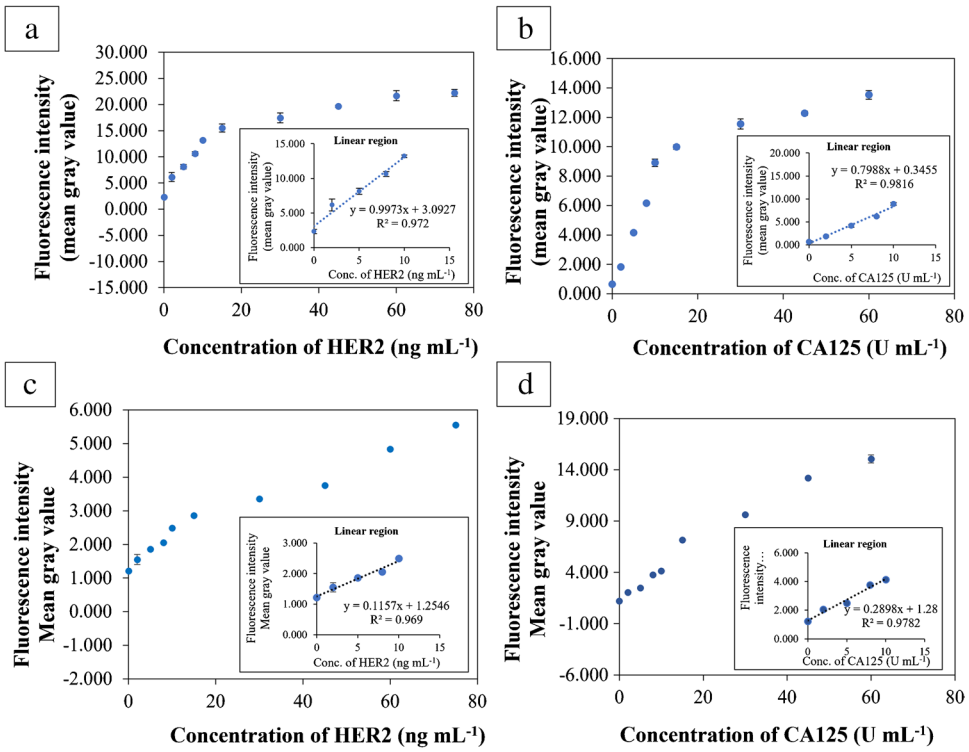

Fig. 2 **a** Calibration curve for the quantitative measurement of HER2 antigen spiked into the serum. **b** Calibration curve for the quantitative measurement of CA125 antigen spiked into the serum. The calibration curve for quantitative measurement of **c** HER2 and **d** CA125 was plotted when two analytes were spiked in simultaneously. Note: The calibration curve was plotted based on the mean gray values obtained from ImageJ software

detecting antibody and presence of the target analyte, were analyzed. No fluorescence signal was observed for any of the 3D porous calcium alginate immuno-beads (Fig. S8). The *p*-value between the two negative control studies was 0.18195, which indicates that there was no non-specific absorption of the detecting antibodies into the 3D porous calcium alginate immuno-bead. Furthermore, the *p*-value affirms the antifouling properties of the blocking buffer (1% Tween-20 in 1 × TBS with 5% $CaCl_2$).

The simultaneous multiplexed detection of HER2 and CA125 antigens spiked into serum samples (*n* = 5)

The assay's multiplexity is important because it improves the accuracy of disease diagnosis, particularly for breast cancer. In simultaneously spiked serum samples, concentrations of 29.2 ng mL^{-1} out of 30 ng mL^{-1} of spiked HER2 and 50 U mL^{-1} out of 50 U mL^{-1} of CA125 proteins were detected, as shown in Fig. S9. For the detection of serum-HER2 and CA125 antigens, replicates had an RSD of 8.2 and 3.5%, respectively, demonstrating that the results were consistent and reproducible.

Precision and recovery test

Intra-day and inter-day precision tests are required for determining the degree of closeness between data obtained within the day and between days to ensure the precision of the method. According to Diaz et al. and Mario et al., test results with an RSD of ≤ 20% are acceptable without the occurrence of false-positive results [66, 67]. As shown in Table S1, the highest RSD obtained from the intra-day result was approximately 17.1%, while the lowest was 1.8%, both of which are acceptable. Furthermore, the high recovery rate of 92% indicates that the results obtained using the 3D porous calcium alginate bead–based assay were accurate and precise. In the inter-day analysis, the performance of the 3D porous calcium alginate immuno-beads in multiplex detection of serum samples spiked with HER2 and CA125 in 25% human serum samples was not significantly different (Fig. S10a and b). Furthermore, RSD values of less than 20% were attained for three consecutive days.

Selectivity and interference test

When single or both target analytes were introduced, the bioreceptors or capturing antibodies were able to capture their respective target analyte, as shown in Fig. S11. When HSA, uric acid, ascorbic acid, and biotin were spiked together with breast cancer biomarkers, the interference test findings presented in Fig. S12a and b revealed no indication of cross-reactivity. The fluorescence intensities of samples spiked with endogenous interference and breast cancer biomarkers were compared to samples spiked with only breast cancer biomarkers. For the four types of interferences stated above, the *p*-values were ($p = 0.898$, 0.924, 0.830, 0.893) for the FITC filter and ($p = 0.650$, 0.563, 0.805, and 0.843) for the

TRITC filter. Endogenous interferences in the serum matrix had no effect on the performance of the 3D porous calcium alginate immuno-bead-based assay when used in simultaneous multiplexed measurement of HER2 and CA125 breast cancer biomarkers, according to these *p*-values. This would enable for the sensitive detection of trace concentrations of breast cancer biomarkers without interference, allowing for early breast cancer diagnosis.

The stability of the 3D porous calcium alginate immuno-bead in multiplex detection of breast cancer biomarkers

The antibodies encapsulated in porous calcium alginate immuno-beads that were stored at 4 °C (Fig. S13a) at room temperature (25 °C) for 14 days were tested to assess the performance stability of the 3D porous calcium alginate immuno-bead (Fig. S13c). After 14 days of storage, the performance of the 3D porous calcium alginate immuno-bead-based test declined non-significantly. When compared to day 1, the beads stored at 4 °C had *p*-values of 0.789 for HER2 detection and 0.892 for CA125 detection. Similarly, *p*-values of 0.712 for HER2 detection and 0.693 for CA125 detection were obtained for beads stored at ambient temperature. As compared to day 1 for both storage conditions, on day 14 of storage at 4 °C, the developed 3D porous calcium alginate immuno-bead-based assay could detect up to 93.9% of spiked HER2, and 99.9% of spiked CA125 in 25% human serum. Similarly, the developed 3D porous immuno-bead-based assay could detect 93.0% of spiked HER2 and 98.1% of spiked CA125 in 25% human serum after 14 days of storage at room temperature. In other words, after 14 days, the 3D porous calcium alginate beads that were stored at room temperature showed slightly lower performance than those stored at 4 °C. The detection of spiked HER2 (spiked 25 ng mL^{-1}, detected 24.78 ng mL^{-1}) and CA125 (spiked 25 U mL^{-1}, detected 24.55 U mL^{-1}) was decreased by 0.9% and 1.8%, respectively. The developed 3D porous calcium alginate bead–based assay was deemed stable after storage in 1 × TBS containing 5% $CaCl_2$ at room temperature due to the insignificant difference in performance between the 3D porous calcium alginate beads that had been stored in the two distinct conditions.

Real sample analysis and method verification

The quantification competency of the developed method was compared to the gold standard, i.e., ELISA for serum-HER2, and CMIA (using an Abbott Architect ci8200 analyzer) for serum CA125 analysis, which was conducted by a BP lab (a commercial laboratory which provides biochemical testing services). The results obtained using the 3D porous calcium alginate immuno-bead assay were consistent with those obtained using standard methods. *p*-values of 0.969 and 0.972 were obtained for serum-HER2 and serum-CA125, respectively, indicating that the results generated by the new approach and standard methods have no significant difference and are equivalent. Furthermore, the analysis took just around 30 min with a single 3D porous calcium alginate bead–based assay, which was much less time than typical ELISA techniques. A performance chart comparing the standard methods and 3D porous calcium

Table 2 A performance comparison was made between standard methods and 3D porous calcium alginate immuno-bead-based assay in clinical serum sample quantification of HER2 and CA125

Patient ID / Method of detection	A	B	C	D	E	F	G	H	I	J
Serum HER2 concentration (ng mL^{-1}) detected by:										
(i) ELISA	18.47	0.32	0.15	0.18	0.48	20.66	0.56	0.17	0.15	0.24
(ii) 3D porous calcium alginate immuno-bead-based assay	18.28	0.34	0.11	0.16	0.50	20.34	0.60	0.18	0.12	0.22
	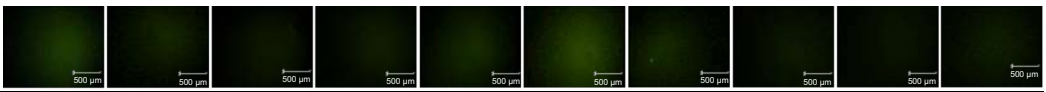									
Serum CA125 concentration (U mL^{-1}) detected by:										
(i) Chemiluminescent Microparticle Immunoassay (CMIA)	21.80	6.40	462.50	66.10	13.20	89.80	11.30	7.50	17.40	13.90
(ii) A single 3D porous calcium alginate immuno-bead-based assay	21.81	6.31	441.94	65.47	13.08	89.45	11.00	7.48	17.29	14.34
	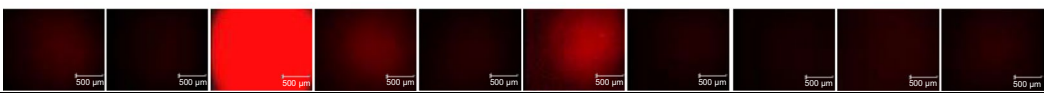									

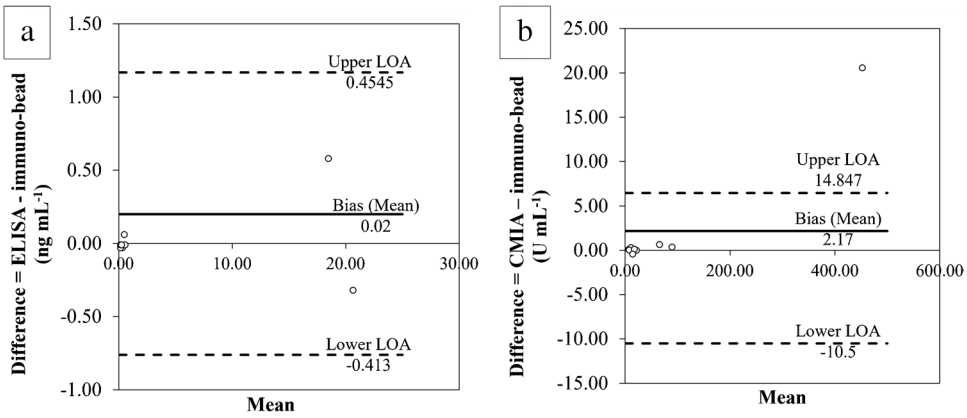

Fig. 3 **a** A Bland–Altman plot was used to compare the methods of ELISA and the 3D porous calcium alginate immuno-bead-based assay in the detection of serum HER2. **b** CMIA and the 3D porous calcium alginate immuno-bead-based assay were compared in the determination of serum CA125

alginate immuno-beads is shown in Table 2. However, the 3D porous calcium alginate immuno-bead-based assay was slightly inferior to the CMIA when it came to detecting very high concentrations of CA125. The difference in the detected concentration beyond the upper limit of agreement (LOA) was 20.56, according to the Bland–Altman plot as shown in Fig. 3. Such a phenomenon could be due to the high intensity of the fluorescence radiation emitted by the 3D porous calcium alginate immuno-bead, which exceeded the readable range and capability of the camera; it could also be attributable to bioreceptor binding saturation inside a single 3D porous calcium alginate immuno-bead. When the concentration is greater than 440 U mL^{-1}, there is no sufficient room for the binding of accessible CA125 proteins and fluorescence tag detecting antibody probes. Nonetheless, because the cutoff concentration for the detection of CA125 is > 30 U mL^{-1}, the detection capabilities of the 3D porous calcium alginate immuno-bead are adequate.

Conclusions

The present study successfully developed a highly sensitive, specific, validated, and relatively rapid early diagnostic approach based on a single 3D porous calcium alginate immuno-bead-based assay for multiplexed breast cancer biomarker detection. The developed approach demonstrates low LOD (0.004 ng mL^{-1} for HER2 and 0.005 U mL^{-1} for CA125 in serum), wide linear range (0–10 ng mL^{-1} and 0–10 U mL^{-1} for the detection of HER2 and CA125, respectively), high precision (1.8–17.1%) and recovery (of more than 92% of HER2 and more than 93% of CA125 in serum spiked samples), good selectivity and negligible interference, high stability at 4 °C and 25 °C, and high sensitivity detection even when real serum samples are examined (below the clinical cutoff value). The obtained results were verified and found to be comparable to those obtained using standard ELISA and CMIA methods, indicating that this approach could be employed in multiplex assays and biosensors. In future work, chemometrics and artificial intelligence (machine learning) will be integrated with the developed approach to demonstrate whether the developed system can deconvolve an unknown mixture outside of any of the pre-measured concentration combinations, in order to make use of the wealth of data that has been collected. It will be interesting to see how this attempt turns out in the future.

Supplementary Information The online version contains supplementary material available at https://doi.org/10.1007/s00216-021-03758-x.

Author contribution Ying Yao Chia: methodology, formal analysis, investigation, writing—original draft, visualization, data curation, software. T. Malathi Thevarajah: resources. Yatimah Alias: resources. Sook Mei Khor: conceptualization, writing—review and editing, supervision, project administration, funding acquisition, resources.

Funding This work was financially supported by the 2019 SATU Joint Research Scheme (JRS) Research Grant (ST003-2019).

Declarations

Conflict of interest The authors declare no competing interests.

Source of biological material The ten archived patient serum samples that were verified to have breast cancer were obtained and aliquoted from University Malaya Medical Center (UMMC) without disclosing any patient information.

References

1. WHO (2021) Breast cancer. WHO. https://www.who.int/news-room/fact-sheets/detail/breast-cancer. Accessed Aug 21 2021
2. CDC (2019) Breast cancer. https://www.cdc.gov/cancer/breast/statistics/index.htm. Accessed Sept 12 2019
3. Shao Y, Yu Y, He Y, Chen Q, Liu H. Serum ATX as a novel biomarker for breast cancer. Medicine (Baltimore). 2019;98(13): e14973. https://doi.org/10.1097/MD.0000000000014973.
4. WHO (2019) Cancer. https://www.who.int/cancer/prevention/diagnosis-screening/breast-cancer/en/. Accessed Jan 10 2019
5. Sharma G, Dave R, Sanadya J, Sharma P, Sharma K. Various types and management of breast cancer: an overview. J Adv Pharm Technol Res. 2010;1(2):109–26.

6. Globocan (2018) Malaysia - Global Cancer Observatory World Health Organization. https://gco.iarc.fr › data › factsheets › populations › 458-malaysia-fact-sheets. Accessed Aug 5 2019
7. Code B (2020) Malaysian Chinese women get most leading cancers. https://codeblue.galencentre.org/2020/01/06/malaysian-chinese-women-get-most-leading-cancers/. Accessed August, 19 2021
8. Society AC (2020) Breast cancer risk and prevention. https://www.cancer.org/content/dam/CRC/PDF/Public/8578.00.pdf.
9. Al-Ajmi K, Lophatananon A, Ollier W, Muir KR. Risk of breast cancer in the UK biobank female cohort and its relationship to anthropometric and reproductive factors. PLoS ONE. 2018;13(7): e0201097. https://doi.org/10.1371/journal.pone.0201097.
10. CDC (2018) Factors that contribute to health disparities in cancer. https://www.cdc.gov/cancer/healthdisparities/basic_info/challenges.htm. Accessed Sept 23 2019
11. Ginsburg O, Yip CH, Brooks A, Cabanes A, Caleffi M, Dunstan Yataco JA, Gyawali B, McCormack V, McLaughlin de Anderson M, Mehrotra R, Mohar A, Murillo R, Pace LE, Paskett ED, Romanoff A, Rositch AF, Scheel JR, Schneidman M, Unger-Saldana K, Vanderpuye V, Wu TY, Yuma S, Dvaladze A, Duggan C, Anderson BO. Breast cancer early detection: a phased approach to implementation. Cancer. 2020;126(Suppl 10):2379–93. https://doi.org/10.1002/cncr.32887.
12. Hakimian F, Ghourchian H, Hashemi A, Arastoo M, Behnam Rad M. Ultrasensitive optical biosensor for detection of miRNA-155 using positively charged Au nanoparticles. Sci Rep. 2018;8(1):2943. https://doi.org/10.1038/s41598-018-20229-z.
13. Wang L (2017) Early diagnosis of breast cancer. Sensors (Basel) 17 (7). https://doi.org/10.3390/s17071572
14. Abrao Nemeir I, Saab J, Hleihel W, Errachid A, Jafferzic-Renault N, Zine N (2019) The advent of salivary breast cancer biomarker detection using affinity sensors. Sensors (Basel) 19 (10). https://doi.org/10.3390/s19102373
15. Hosseini S, Vázquez-Villegas P, Rito-Palomares M, Martinez-Chapa SO (2018) Advantages, disadvantages and modifications of conventional ELISA. In: Enzyme-linked immunosorbent assay (ELISA): From A to Z. Springer Singapore, Singapore, pp 67–115. https://doi.org/10.1007/978-981-10-6766-2_5
16. Jeong MS, Ahn DR. A microwell plate-based multiplex immunoassay for simultaneous quantitation of antibodies to infectious viruses. Analyst. 2015;140(6):1995–2000. https://doi.org/10.1039/c4an02262a.
17. Roh YH, Lee HJ, Kim JY, Kim HU, Kim SM, Bong KW. Precipitation-based colorimetric multiplex immunoassay in hydrogel particles. Lab Chip. 2020;20(16):2841–50. https://doi.org/10.1039/d0lc00325e.
18. Valm AM, Oldenbourg R, Borisy GG. Multiplexed spectral imaging of 120 different fluorescent labels. PLoS ONE. 2016;11(7): e0158495. https://doi.org/10.1371/journal.pone.0158495.
19. Altintas Z, Tothill I. Biomarkers and biosensors for the early diagnosis of lung cancer. Sensors and Actuators B-Chemical. 2013;188:988–98. https://doi.org/10.1016/j.snb.2013.07.078.
20. Bhatt A, Mathur R, Farooque A, Verma A, Dwarakanath B. Cancer biomarkers - current perspectives. Indian J Med Res. 2010;132:129–49.
21. Li H, DeSouza LV, Ghanny S, Li W, Romaschin AD, Colgan TJ, Siu KW. Identification of candidate biomarker proteins released by human endometrial and cervical cancer cells using two-dimensional liquid chromatography/tandem mass spectrometry. J Proteome Res. 2007;6(7):2615–22. https://doi.org/10.1021/pr070798.
22. Wagner MK, Li F, Li J, Li XF, Le XC. Use of quantum dots in the development of assays for cancer biomarkers. Anal Bioanal Chem. 2010;397(8):3213–24. https://doi.org/10.1007/s00216-010-3847-9.
23. Coulter B (2015) Tumour markers clinical aspects. http://immunotech.cz/Media/Default/Page/Tumor_markers_Clinical_asp.pdf. Accessed May 30 2020
24. Yager P, Domingo GJ, Gerdes J. Point-of-care diagnostics for global health. Annu Rev Biomed Eng. 2008;10:107–44. https://doi.org/10.1146/annurev.bioeng.10.061807.160524.
25. Nagpal M, Singh S, Singh P, Chauhan P, Zaidi MA. Tumor markers: a diagnostic tool. National journal of maxillofacial surgery. 2016;7(1):17–20. https://doi.org/10.4103/0975-5950.196135.
26. Cibele G (2011) Biosensors for health applications. Biosensors for Health, Environment and Biosecurity. Pier Andrea Serra, IntechOpen. https://doi.org/10.5772/16983
27. Prittesh P, Jainish P. Biosensors and biomarkers: promising tools for cancer diagnosis. Biosens Bioelectron. 2017;3(4):313–6. https://doi.org/10.15406/ijbsbe.2017.03.00072.
28. Szunerits S, Boukherroub R. Graphene-based biosensors. Interface. Focus. 2018;8(3):20160132. https://doi.org/10.1098/rsfs.2016.0132.
29. Padmanabhan S, Shinoj VK, Murukeshan VM, Padmanabhan P. Highly sensitive optical detection of specific protein in breast cancer cells using microstructured fiber in extremely low sample volume. J Biomed Opt. 2010;15(1): 017005. https://doi.org/10.1117/1.3302810.
30. Wang Z, Chen Q, Zhong Y, Yu X, Wu Y, Fu F. A multicolor immunosensor for sensitive visual detection of breast cancer biomarker based on sensitive NADH-ascorbic-acid-mediated growth of gold nanobipyramids. Anal Chem. 2020;92(1):1534–40. https://doi.org/10.1021/acs.analchem.9b04828.
31. Salama O, Herrmann S, Tziknovsky A, Piura B, Meirovich M, Trakht I, Reed B, Lobel LI, Marks RS. Chemiluminescent optical fiber immunosensor for detection of autoantibodies to ovarian and breast cancer-associated antigens. Biosens Bioelectron. 2007;22(7):1508–16. https://doi.org/10.1016/j.bios.2006.07.003.
32. John TG, Paul SD, Xudong F. Detection of HER2 breast cancer biomarker using the opto-fluidic ring resonator biosensor. Sens Actuators, B Chem. 2010;146(1):226–30.
33. Zhu H, Dale PS, Caldwell CW, Fan X. Rapid and label-free detection of breast cancer biomarker CA15-3 in clinical human serum samples with optofluidic ring resonator sensors. Anal Chem. 2009;81(24):9858–65. https://doi.org/10.1021/ac902437g.
34. Sun D, Ran Y, Wang G (2017) Label-free detection of cancer biomarkers using an in-line taper fiber-optic interferometer and a fiber Bragg grating. Sensors (Basel) 17 (11). https://doi.org/10.3390/s17112559
35. Monteiro JP, Predabon SM, Bonafe EG, Martins AF, Brolo AG, Radovanovic E, Girotto EM. SPR platform based on image acquisition for HER2 antigen detection. Nanotechnology. 2017;28(4): 045206. https://doi.org/10.1088/1361-6528/28/4/045206.
36. Elakkiya V, Menon MP, Nataraj D, Biji P, Selvakumar R (2017) Optical detection of CA 15.3 breast cancer antigen using CdS quantum dot. IET Nanobiotechnol 11 (3):268–276. https://doi.org/10.1049/iet-nbt.2016.0012
37. Zheng Z, Wu L, Li L, Zong S, Wang Z, Cui Y. Simultaneous and highly sensitive detection of multiple breast cancer biomarkers in real samples using a SERS microfluidic chip. Talanta. 2018;188:507–15. https://doi.org/10.1016/j.talanta.2018.06.013.
38. Satvinder P, Xuan W, Suresh N. Toward point-of-care diagnostics of breast cancer: development of an optical biosensor using quantum dots. IEEE Sensors Letters. 2017;1(4):1–4.
39. Liu B, Zhang D, Ni H, Wang D, Jiang L, Fu D, Han X, Zhang C, Chen H, Gu Z, Zhao X. Multiplex analysis on a single porous hydrogel bead with encoded SERS nanotags. ACS Appl Mater Interfaces. 2018;10(1):21–6. https://doi.org/10.1021/acsami.7b14942.
40. Piao Y, Liu F, Seo TS. A novel molecular beacon bearing a graphite nanoparticle as a nanoquencher for in situ mRNA detection

in cancer cells. ACS Appl Mater Interfaces. 2012;4(12):6785–9. https://doi.org/10.1021/am301976r.
41. Saeed AA, Sanchez JLA, O'Sullivan CK, Abbas MN. DNA biosensors based on gold nanoparticles-modified graphene oxide for the detection of breast cancer biomarkers for early diagnosis. Bioelectrochemistry. 2017;118:91–9. https://doi.org/10.1016/j.bioelechem.2017.07.002.
42. Selwyna PG, Loganathan P, Begam K (2013) Development of electrochemical biosensor for breast cancer detection using gold nanoparticle doped CA 15–3 antibody and antigen interaction. Paper presented at the International Conference on Signal Processing, Image Processing & Pattern Recognition, Coimbatore, India, February
43. Yazdanparast S, Benvidi A, Banaei M, Nikukar H, Tezerjani MD, Azimzadeh M. Dual-aptamer based electrochemical sandwich biosensor for MCF-7 human breast cancer cells using silver nanoparticle labels and a poly(glutamic acid)/MWNT nanocomposite. Mikrochim Acta. 2018;185(9):405. https://doi.org/10.1007/s00604-018-2918-z.
44. Salahandish R, Ghaffarinejad A, Naghib SM, Majidzadeh AK, Zargartalebi H, Sanati-Nezhad A. Nano-biosensor for highly sensitive detection of HER2 positive breast cancer. Biosens Bioelectron. 2018;117:104–11. https://doi.org/10.1016/j.bios.2018.05.043.
45. Akbari N, Khalilzadeh B, Samadi Pakchin P, Saber R, Ghahremani M, Omidi Y. A highly sensitive and reliable detection of CA15-3 in patient plasma with electrochemical biosensor labeled with magnetic beads. Biosens Bioelectron. 2018;122:8–15. https://doi.org/10.1016/j.bios.2018.08.047.
46. Huerta-Nunez L, Gutierrez-Iglesias G, Martinez-Cuazitl A, Mata-Miranda M, Alvarez-Jimenez V, Sanchez-Monroy V, Golberg A, Gonzalez-Diaz C. A biosensor capable of identifying low quantities of breast cancer cells by electrical impedance spectroscopy. Sci Rep. 2019;9(1):6419. https://doi.org/10.1038/s41598-019-42776-9.
47. Singh RD, Shandilya R, Bhargava A, Kumar R, Tiwari R, Chaudhury K, Srivastava RK, Goryacheva IY, Mishra PK. Quantum dot based nano-biosensors for detection of circulating cell free miRNAs in lung carcinogenesis: from biology to clinical translation. Front Genet. 2018;9:616. https://doi.org/10.3389/fgene.2018.00616.
48. Ma H, Yan T, Zhang Y, Gao P, Pang X, Du B, Wei Q. A biomimetic mussel-inspired photoelectrochemical biosensing chip for the sensitive detection of CD146. Analyst. 2015;140(15):5019–22. https://doi.org/10.1039/c5an00873e.
49. Abril E, Lizbeth BG, Olimpia S, Dulce V, Jacqueline O, Kevin G, Lázaro H, Joaquín O. Development of AlN thin films for breast cancer acoustic biosensors. J Market Res. 2019;8(1):350–8. https://doi.org/10.1016/j.jmrt.2018.02.007.
50. Putzbach W, Ronkainen NJ. Immobilization techniques in the fabrication of nanomaterial-based electrochemical biosensors: a review. Sensors (Basel). 2013;13(4):4811–40. https://doi.org/10.3390/s130404811.
51. Barberi J, Spriano S (2021) Titanium and protein adsorption: an overview of mechanisms and effects of surface features. Materials (Basel) 14 (7). https://doi.org/10.3390/ma14071590
52. Chen KJH, Zhang D, Lee KH, Cangelosi GA, Soelberg SD, Furlong CE, Chung JH, Shen AQ. Microfluidic one-step synthesis of alginate microspheres immobilized with antibodies. J R Soc Interface. 2013;10(88):20130566. https://doi.org/10.1098/rsif.2013.0566.
53. Chikkaveeraiah B, Bhirde A, Morgan N, Eden H, Chen X. Electrochemical immunosensors for detection of cancer protein biomarkers. ACS Nano. 2012;6(8):6546–61. https://doi.org/10.1021/nn3023969.
54. Krishnendu S, Sarit SA, Chaekyu K, Xiaoning L, Vincent MR. Gold nanoparticles in chemical and biological sensing. Chem Rev. 2012;112(5):2739–79.
55. Chen D, Zhang M, Zhou F, Hai H, Li J. Ultrasensitive electroluminescence biosensor for a breast cancer marker microRNA based on target cyclic regeneration and multi-labeled magnetized nanoparticles. Mikrochim Acta. 2019;186(9):628. https://doi.org/10.1007/s00604-019-3719-8.
56. Lu W, Arumugam SR, Senapati D, Singh AK, Arbneshi T, Khan SA, Yu H, Ray PC. Multifunctional oval-shaped gold-nanoparticle-based selective detection of breast cancer cells using simple colorimetric and highly sensitive two-photon scattering assay. ACS Nano. 2010;4(3):1739–49. https://doi.org/10.1021/nn901742q.
57. Kaklamani G, Kazaryan D, Bowen J, Iacovella F, Anastasiadis S, Deligeorgis G. On the electrical conductivity of alginate hydrogels. Regen Biomater. 2018;5(5):293–301. https://doi.org/10.1093/rb/rby019.
58. Shoichet MS, Li RH, White ML, Winn SR. Stability of hydrogels used in cell encapsulation: an in vitro comparison of alginate and agarose. Biotechnol Bioeng. 1996;50:374–81. https://doi.org/10.1002/(SICI)1097-0290(19960520)50:4%3c374::AID-BIT4%3e3.0.CO;2-I (**PMID: 18626986**).
59. Herrmann A, Haag R, Schedler U. Hydrogels and their role in biosensing applications. Adv Healthc Mater. 2021;10(11): e2100062. https://doi.org/10.1002/adhm.202100062.
60. Chen KCJ, Yen KC, Hsieh HC, Sun JS, Lin FH. 3D porous calcium-alginate scaffolds cell culture system improved human osteoblast cell clusters for cell therapy. Theranostics. 2015;5(6):643–55. https://doi.org/10.7150/thno.11372.
61. Agnieszka K. Alginate-based hydrogels in regenerative medicine. Alginates - Recent Uses of This Natural Polymer, Leonel Pereira, IntechOpen. 2019. https://doi.org/10.5772/intechopen.88258.
62. Baskic D, Ristic P, Pavlovic S, Arsenijevic N. Serum HER2 and CA 15–3 in breast cancer patients. J BUON. 2004;9(3):289–94.
63. Ahmed MK. Tumor markers of breast cancer: new prospectives. Journal of Oncological Sciences. 2017;3(1):5–11. https://doi.org/10.1016/j.jons.2017.01.001.
64. Fang C, Cao Y, Liu X, Zeng XT, Li Y. Serum CA125 is a predictive marker for breast cancer outcomes and correlates with molecular subtypes. Oncotarget. 2017;8(38):63963–70. https://doi.org/10.18632/oncotarget.19246.
65. Nadia TD, Yatimah A, Sook MK. Indium tin oxide with zwitterionic interfacial design for biosensing applications in complex matrices. Appl Surf Sci. 2015;325:91–9.
66. Diaz DA, Colgan ST, Langer CS, Bandi NT, Likar MD, Van Alstine L. Dissolution similarity requirements: how similar or dissimilar are the global regulatory expectations? AAPS J. 2016;18(1):15–22. https://doi.org/10.1208/s12248-015-9830-9.
67. Mario L, Rocci J, Stephen L. Regulated bioanalysis: fundamentals and practice. Advances in the Pharmaceutical Sciences Series. 2017;26:123.